

Selectivity of the Nucleon Induced Deuteron Breakup and Relativistic Effects

H. Witala, J. Golak, and R. Skibiński
Institute of Physics, Jagiellonian University, PL-30059 Cracow, Poland
(Dated: August 16, 2018)

Theoretical predictions for the nucleon induced deuteron breakup process based on solutions of the three-nucleon Faddeev equation including such relativistic features as the relativistic kinematics and boost effects are presented. Large changes of the breakup cross section in some complete configurations are found at higher energies. The predicted relativistic effects, which are mostly of dynamical origin, seem to be supported by existing data.

PACS numbers: 21.30.-x, 21.45.+v, 24.10.-i, 24.70.+s

Recent studies of elastic nucleon-deuteron (Nd) scattering and nucleon induced deuteron breakup revealed a number of cases where the nonrelativistic description based only on pairwise nucleon-nucleon (NN) forces is insufficient to explain the three-nucleon (3N) data. This happens in spite of the fact, that these high precision NN potentials describe very well the NN data set to about 350 MeV laboratory energy. Those findings extended exploration of the properties of three-nucleon forces (3NFs) to the reactions in the 3N continuum. Such forces appear for the first time in the 3N system where they provide an additional contribution to a predominantly pairwise potential energy of three nucleons. Generally speaking, the studied discrepancies between a theory based only on NN potentials and experiment become larger for increasing energy of the 3N system. Adding a 3N force to the pairwise interactions leads in some cases to a better description of the data. The best studied example is the discrepancy for the elastic angular distribution in the region of its minimum and at backward angles [1, 2, 3]. This clear discrepancy can be removed at energies below ≈ 100 MeV by adding modern 3NFs to the nuclear Hamiltonian. Such a 3NF, mostly of the 2π -exchange character, must be adjusted individually with each NN potential to the experimental binding energy of ${}^3\text{H}$ and ${}^3\text{He}$. At energies higher than ≈ 100 MeV current 3NFs improve only partially the description of cross section data and the remaining discrepancies, which increase with energy, indicate the possibility of relativistic effects. The need for a relativistic description of 3N scattering was also raised when precise measurements of the total cross section for neutron-deuteron (nd) interaction [4] were analyzed within the framework of the nonrelativistic Faddeev calculations [5]. Also there the NN forces alone were insufficient to describe the data above ≈ 100 MeV. The effects due to relativistic kinematics considered in ref. [5] were comparable at higher energies to the effects due to 3NFs. This demonstrates the importance of a study taking relativistic effects in the 3N continuum into account.

Recently first results of relativistic 3N Faddeev calculations for the elastic Nd scattering have become available [6]. The relativistic formulation applied was of the instant form of relativistic dynamics [7]. A starting point of this formulation for 3N scattering is the

Lorentz boosted NN potential $V(\vec{k}, \vec{k}'; \vec{P})$ which generates the two-nucleon (2N) boosted t matrix $t(\vec{k}, \vec{k}'; \vec{P})$ in a moving frame via a standard relativistic 2N Lippmann-Schwinger equation

$$t(\vec{k}, \vec{k}'; \vec{P}) = V(\vec{k}, \vec{k}'; \vec{P}) + \int d^3 k'' \frac{V(\vec{k}, \vec{k}''; \vec{P}) t(\vec{k}'', \vec{k}'; \vec{P})}{\sqrt{(2\omega(\vec{k}'))^2 + \vec{P}^2} - \sqrt{(2\omega(\vec{k}''))^2 + \vec{P}^2} + i\epsilon}. \quad (1)$$

The NN potential in an arbitrary moving frame $V(\vec{P})$ is obtained from the interaction v defined in the two-nucleon c.m. system by [8]

$$V(\vec{P}) \equiv \sqrt{(2\omega(\vec{k}) + v)^2 + \vec{P}^2} - \sqrt{(2\omega(\vec{k}))^2 + \vec{P}^2}. \quad (2)$$

The relativistic kinetic energy of three equal mass (m) nucleons in their c.m. system can be expressed by the relative momentum \vec{k} in one of the two-body subsystems and momentum of the third nucleon \vec{q} (the total momentum of the two-body subsystem is then $\vec{P} = -\vec{q}$) as

$$H_0 = \sqrt{(2\omega(\vec{k}))^2 + \vec{q}^2} + \sqrt{m^2 + \vec{q}^2}, \quad (3)$$

where $2\omega(\vec{k}) \equiv 2\sqrt{m^2 + \vec{k}^2}$ is the momentum dependent 2N mass operator.

The Nd scattering with neutrons and protons interacting through a NN potential V alone is described in terms of a breakup operator T satisfying the Faddeev-type integral equation [9, 10]

$$T|\phi\rangle = tP|\phi\rangle + tPG_0T|\phi\rangle. \quad (4)$$

The permutation operator $P = P_{12}P_{23} + P_{13}P_{23}$ is given in terms of the transpositions P_{ij} , which interchange nucleons i and j. The incoming state $|\phi\rangle \equiv |\vec{q}_0\rangle |\phi_d\rangle$ describes the free nucleon-deuteron motion with the relative momentum \vec{q}_0 and the deuteron wave function $|\phi_d\rangle$. The $G_0 \equiv \frac{1}{E + i\epsilon - H_0}$ is the free 3N propagator with total 3N c.m. energy E expressed in terms of the initial neutron momentum \vec{q}_0 relative to the deuteron

$$E = \sqrt{(M_d)^2 + \vec{q}_0^2} + \sqrt{m^2 + \vec{q}_0^2}, \quad (5)$$

where M_d is the deuteron rest mass.

The transition operators for elastic scattering, U , and breakup, U_0 , are given in terms of T by [9, 10]

$$\begin{aligned} U &= PG_0^{-1} + PT \\ U_0 &= (1 + P)T. \end{aligned} \quad (6)$$

The state $U_0|\phi\rangle$ is projected onto the state $|\phi_0\rangle$ which describes the free motion of the three outgoing nucleons in the 3N c.m. system in terms of the relative momentum of the 2N subsystem $\vec{k}_{3N \text{ c.m.}}(2-3)$, defined in the 3N c.m., and momentum of the spectator nucleon \vec{q} defined above: $|\phi_0\rangle \equiv |\vec{k}_{3N \text{ c.m.}}(2-3) \vec{q}\rangle_1$. This leads to the breakup transition amplitude

$$\langle \phi_0 | U_0 | \phi \rangle = \sum_i \langle \vec{k}_{3N \text{ c.m.}}(j-k) \vec{q}_i | T | \phi \rangle. \quad (7)$$

The choice of the relative momentum \vec{k} in the NN c.m. subsystem and the momentum \vec{q} of the spectator nucleon in the 3N c.m. system to describe configuration of three nucleons is the most convenient in the relativistic case. In the nonrelativistic limit the momentum \vec{k} reduces to the standard Jacobi momentum \vec{p} [10]. To solve Eq.(4) numerically partial wave decomposition is still required. The standard partial wave states $|pq\alpha\rangle \equiv |pq(ls)j(\lambda\frac{1}{2})IJ(t\frac{1}{2})T\rangle$ [10], however, are generalized in the relativistic case due to the choice of the NN-subsystem momentum \vec{k} and the total spin s both defined in the NN c.m. system. This lead to Wigner spin rotations when boosting to the 3N c.m. system [6, 7], resulting in a more complex form for the permutation matrix element [6] than used in the nonrelativistic case [10]. A restricted relativistic calculation with $j < 2$ partial wave states showed that Wigner spin rotations have only negligible effects [6]. Due to this we neglected the Wigner rotations completely in the present study. To achieve converged results at energies up to ≈ 250 MeV all partial wave states with total angular momenta of the 2N subsystem up to $j \leq 5$ have to be used and all total angular momenta of the 3N system up to $J = 25/2$ taken into account. This leads to a system of up to 143 coupled integral equations in two continuous variables for a given total angular momentum J and total parity $\pi = (-)^{l+\lambda}$ of the 3N system. For the details of our relativistic formulation and of the numerical performance in the relativistic and nonrelativistic cases we refer to Ref. [6, 9, 10].

In the present study we applied as a dynamical input a relativistic interaction v generated from the nonrelativistic NN potential CDBonn [11] according to the analytical prescription of ref. [12]. This analytical transformation allows to obtain an exactly on-shell equivalent to the CDBonn relativistic potential v which provides the corresponding relativistic t matrix. The boosted potential was not treated in all its complexity as given in ref. [13] but a restriction to the leading order term in a P/ω and v/ω expansion was made

$$V(\vec{k}, \vec{k}'; \vec{P}) = v(\vec{k}, \vec{k}')$$

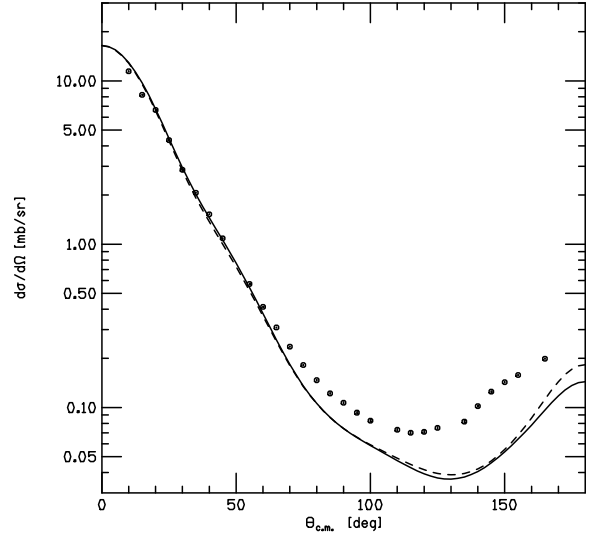


FIG. 1: Differential cross section for elastic Nd scattering at 250 MeV. The dashed and solid lines are the results of the relativistic and nonrelativistic Faddeev calculations based on the NN potential CDBonn. The pd data are from [19].

$$\times \left[1 - \frac{\vec{P}^2}{8\sqrt{m^2 + \vec{k}^2} \sqrt{m^2 + (\vec{k}')^2}} \right]. \quad (8)$$

The quality of such an approximation has been checked by calculating the deuteron wave function $\phi_d(\vec{k})$ of the deuteron moving with momentum \vec{P} for a number of values corresponding to incoming nucleon lab. energy ≤ 250 MeV. The resulting deuteron binding energies and the deuteron D-state probabilities for the deuteron in motion are close to the values for the deuteron at rest.

In Fig. 1 we show the nucleon angular distribution for elastic nucleon-deuteron scattering at $E_{lab}^N = 250$ MeV. It is seen that, like in a study of Nd elastic scattering in ref. [6] where the AV18 [14] NN potential instead of CDBonn have been used, relativistic effects for the cross section are restricted only to the backward angles where relativity increases the nonrelativistic cross section. At other angles the effects are small. In spite of the fact that the relativistic phase-space factor increases with energy faster than the nonrelativistic one (at 250 MeV their ratio amounts to 1.175), the relativistic nuclear matrix element outweighs this increase and leads for the cross section in a wide angular range to a relatively small relativistic effect.

The breakup reaction with three free outgoing nucleons in the final state provides a unique possibility to access the matrix elements of the breakup operator T with specific values of momenta $|\vec{k}|$ and $|\vec{q}|$ in a pointwise manner. Each exclusive breakup configuration specified completely by 3N c.m. momenta \vec{k}_i of outgoing nucleons requires three matrix elements ${}_i \langle \vec{k}(\vec{k}_j, \vec{k}_k), \vec{q} = \vec{k}_i | T | \phi \rangle$ with $(i, j, k) = (1, 2, 3)$ and cyclical permutations, and \vec{k}

and \vec{q} providing the total 3N c.m. energy

$$E = \sqrt{4(m^2 + \vec{k}^2) + \vec{q}^2} + \sqrt{m^2 + \vec{q}^2}. \quad (9)$$

This is entirely different from the elastic scattering where, due to continuum momentum distribution of nucleons inside the deuteron a broad range of $|\vec{k}|$ - and $|\vec{q}|$ -values contributes to the elastic scattering transition matrix element. That particular selectivity of the breakup singles out this reaction as a tool to look for localized effects which when averaged are difficult to see in elastic scattering.

This selectivity of breakup helps to reveal relativistic effects in the 3N continuum. Even at relatively low incoming nucleon energy $E_{lab}^N = 65$ MeV they can be clearly seen in cross sections of some exclusive breakup configurations as exemplified in Figs. 2 and 3. For the configuration of Fig. 2 the angles of the two outgoing protons detected in coincidence were chosen in such a way that for the arc-length $S \approx 30$ MeV all three nucleons have equal momenta which in the 3N c.m. system lie in the plane perpendicular to the beam direction (symmetrical space star (SSS) condition). For the configuration from Fig. 3 at the value of $S \approx 46$ MeV the third, not observed nucleon is at rest in lab. system (quasi-free scattering (QFS) geometry). In these two breakup configurations the inclusion of relativity lowers the cross section: by $\approx 8\%$ in the case of SSS and by $\approx 10\%$ in the case of QFS. In the lower parts of Figs. 2 and 3 contributions to this effect due to kinematics and dynamics are shown. The five-fold differential cross section can be written as

$$\frac{d^5\sigma}{d\Omega_1 d\Omega_2 dS} = \left(\sum_{m_{in}, m_{out}} | \langle \phi_0 | U_0 | \phi \rangle |^2 \right) \rho_{kin}, \quad (10)$$

with the kinematical factor ρ_{kin} containing the phase-space factor and the initial flux. The transition probability for breakup $| \langle \phi_0 | U_0 | \phi \rangle |^2$, averaged over the initial m_{in} and summed over final m_{out} sets of particles spin projections, forms the dynamical part of the cross section. In the lower parts of figures the ratio of the relativistic to the nonrelativistic kinematical factor $\rho_{kin}^{rel}/\rho_{kin}^{nrel}$ as a function of S is shown by the dashed line. The corresponding ratio for the dynamical parts of the cross section is shown by the solid line. As seen in Fig. 3 for the QFS configuration the whole effect is due to a dynamical change of the transition matrix element. For this configuration the nonrelativistic and relativistic kinematical factors are practically equal for large region of S -values (see Fig. 3). For SSS about 30% of the total effect is due to a decrease of the relativistic kinematical factor with respect to the nonrelativistic one (see Fig. 2).

The cross sections in these particular configurations are rather stable with respect to exchange between modern NN forces, combining them or not with three-nucleon forces [15]. Due to that relativistic effects seem to explain the small and up to now puzzling overestimation of the 65 MeV SSS cross section data [16] by modern nuclear

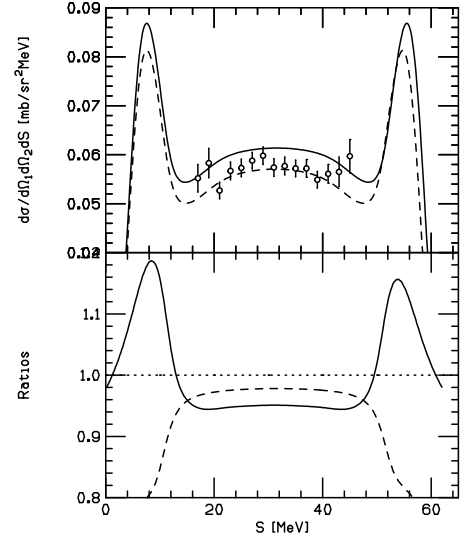


FIG. 2: Five-fold differential cross section $d^5\sigma/d\Omega_1 d\Omega_2 dS$ as a function of arc-length S for the SSS configuration (see text) of $d(p,pp)n$ reaction at 65 MeV. The lab. angles of the outgoing protons are $\theta_1 = \theta_2 = 54^\circ$ and $\phi_{12} = 120^\circ$. The solid and dashed lines are the results of the nonrelativistic and relativistic Faddeev calculations based on the NN potential CDBonn. The 65 MeV pd data are from [16]. The lower part shows the ratios of the relativistic and nonrelativistic phase-space factors (dashed line) and of the cross sections divided by the corresponding phase-space factor (solid line).

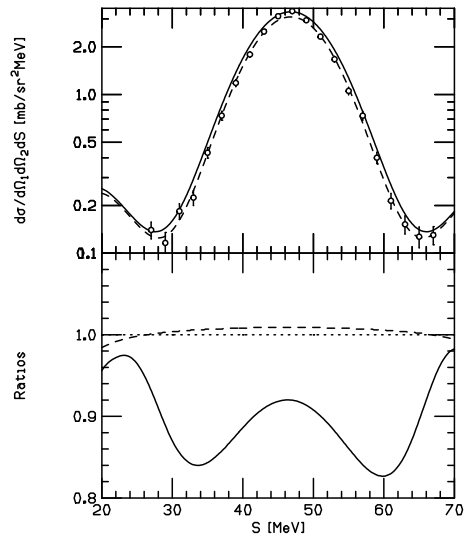


FIG. 3: The same as in Fig. 2 for the QFS geometry (see text). The lab. angles of the outgoing protons are $\theta_1 = \theta_2 = 44^\circ$ and $\phi_{12} = 180^\circ$. The 65 MeV pd data are from [17].

forces and can account for the experimental width of this QFS peak [17].

At higher energies selectivity of breakup allows us to find the configurations with significantly larger relativistic effects. In Fig. 4 this is exemplified at $E_{lab}^N = 200$ MeV and the predicted effects of up to $\approx 60\%$, which are

mostly of dynamical origin, seem to be supported by the data of ref. [18].

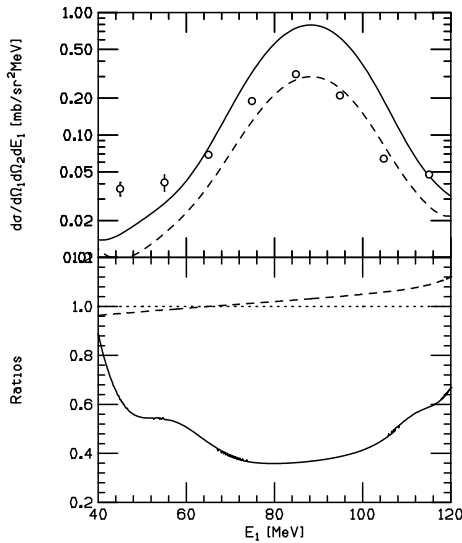


FIG. 4: Five-fold differential cross section $d^5\sigma/d\Omega_1 d\Omega_2 dE_1$ as a function of energy of the detected proton E_1 for $d(p, pn)p$ reaction at 200 MeV. The polar lab. angle of the outgoing proton and neutron is $\theta_1 = 52^\circ$ and $\theta_2 = 45^\circ$, respectively. The azimuthal angle $\phi_{12} = 180^\circ$. For the description of lines and the bottom part see Fig. 2. The data are from [18].

The selectivity of complete breakup is gradually lost when uncomplete reactions are considered. In the total nd breakup cross section the effects disappear. Integrating over all available complete breakup configurations provides nearly equal relativistic (90.25 mb at 65 MeV and 43.37 mb at 250 MeV) and nonrelativistic (91.12 mb

and 45.41 mb) total breakup cross sections. Also integrated elastic scattering angular distribution (71.25 mb and 9.33 mb - relativistic, and 71.40 mb and 9.57 mb - nonrelativistic) and the total cross section for the nd interaction do not reveal significant relativistic effects. This shows, that the discrepancies between theory and data found in previous studies at higher energies for the total cross section and elastic scattering angular distributions, which remain even after combining NN potentials with 3NFs, have to result from additional contributions to the 3N force, which have different than the 2π -exchange character.

Summarizing, we showed that selectivity of the complete breakup reaction enables us to reveal in 3N continuum clear signals from relativistic effects. Existing breakup data seem to support the predicted effects, when the relativity is included in the instant form of relativistic dynamics as proposed by Bakamjian and Thomas. Precise complete breakup data at energies around 200 MeV are welcome to further test these predictions. The QFS breakup configurations due to their large cross sections and insensitivity to the details of nuclear forces are favored for this purpose.

This work was supported by the Polish Committee for Scientific Research under Grant No. 2P03B00825 and by the Japan Society for the Promotion of Science. HW would like to thank for hospitality and support during the stay at RCNP, Japan and at TUNL, USA. The numerical calculations have been performed on the CRAY SV1 and on the IBM Regatta p690+ of the NIC in Jülich, Germany.

[1] H. Witala *et al.*, Phys. Rev. Lett. **81**, 1183 (1998).
[2] K. Sekiguchi *et al.*, Phys. Rev. C**65**, 034003 (2002).
[3] H. Witala *et al.*, Phys. Rev. C**63**, 024007 (2001).
[4] W.P. Abfalterer *et al.*, Phys. Rev. Lett. **81**, 57 (1998).
[5] H. Witala *et al.*, Phys. Rev. C**59**, 3035 (1999).
[6] H. Witala *et al.*, Phys. Rev. C**71**, 054001 (2005).
[7] B. D. Keister and W. N. Polyzou, Adv. Nucl. Phys. **20**, 225 (1991).
[8] F. Coester, Helv. Phys. Acta **38**, 7 (1965).
[9] H. Witala *et al.*, Few-Body Syst. **3**, 123 (1988).
[10] W. Glöckle *et al.*, Phys. Rep. **274**, 107 (1996).
[11] R. Machleidt, Phys. Rev. C **63**, 024001 (2001).
[12] H. Kamada, and W. Glöckle, Phys. Rev. Lett. **80**, 2547 (1998).
[13] H. Kamada *et al.*, Phys. Rev. C **66**, 044010 (2002).
[14] R. B. Wiringa *et al.*, Phys. Rev. C **51**, 38 (1995).
[15] J. Kuroś-Żołnierczuk *et al.*, Phys. Rev. C**66**, 024004 (2002).
[16] J. Zejma *et al.*, Phys. Rev. C**55**, 42 (1997).
[17] M. Allet *et al.*, Few-Body Syst. **20**, 27 (1996).
[18] W. Pairsuwan *et al.*, Phys. Rev. C**52**, 2552 (1995).
[19] K. Hatanaka *et al.*, Phys. Rev. C **66**, 044002 (2002).